Investigating the Effect of Microbial Activity and Chemical Concentrations on the Mineralogy and Morphology of Ureolytic Bio-Cementation

Robert J. Burdalski¹ and Michael G. Gomez²

¹Graduate Student, Dept. of Civil and Environmental Engineering, Univ. of Washington, Seattle, WA. E-mail: rjb360@uw.edu

²Assistant Professor, Dept. of Civil and Environmental Engineering, Univ. of Washington, Seattle, WA. E-mail: mggomez@uw.edu

ABSTRACT

Numerous laboratory studies in the past decade have demonstrated the ability of microbially induced calcite precipitation (MICP), a bio-mediated soil improvement method, to favorably transform a soil's engineering properties including increased shear strength and stiffness with reductions in hydraulic conductivity and porosity. Despite significant advances in treatment application techniques and characterization of post-treatment engineering properties, relationships between biogeochemical conditions during precipitation and post-treatment material properties have remained poorly understood. Bacterial augmentation, stimulation, and cementation treatments can vary dramatically in their chemical constituents, concentrations, and ratios between researchers, with specific formulas oftentimes perpetuating despite limited understanding of their engineering implications. In this study, small-scale batch experiments were used to systematically investigate how biogeochemical conditions during precipitate synthesis may influence resulting bio-cementation and related material engineering behaviors. Aqueous solution chemistry was monitored in time to better understand the relationship between the kinetics of ureolysis and calcium carbonate precipitation, and resulting precipitates. Following all experiments, precipitates were evaluated using x-ray diffraction and scanning electron microscopy to characterize mineralogy and morphology. Results obtained from these investigations are expected to help identify the primary chemical and biological factors during synthesis that may control bio-cementation material properties and influence engineering performance aspects including long-term resilience.

INTRODUCTION

Bio-mediated soil improvement is an emerging field in geotechnical engineering with the potential to develop technologies that can improve the engineering properties of soils with reductions in environmental impacts (DeJong et al. 2013). Recently researchers have examined a process known as Microbially Induced Calcite Precipitation (MICP), which uses biologically mediated urea hydrolysis [Eq. (1)] in the presence of soluble calcium to enable precipitation of calcium carbonate on soil particle surfaces and contacts (Stocks-Fischer et al. 1999; DeJong et al. 2006).

$$CO(NH_2)_2 + 2H_2O \rightarrow 2NH_3 + H_2CO_3$$
 [Eq. (1)]

MICP can transform the engineering properties of soils through increases in shear stiffness and strength with reductions in hydraulic conductivity and porosity (DeJong et al. 2006; Gomez et al. 2018a). The technology has potential engineering applications spanning liquefaction mitigation, slope stability improvement, subsurface flow manipulation, and contaminant immobilization among others (Fujita et al. 2004; DeJong et al. 2006; Montoya et al. 2013; Minto et al. 2016). Despite recent advances with respect to application techniques (O'Donnell et al.

2017; Gomez et al. 2018b), up-scaling the process to meter-scale (van Paassen et al. 2011; Gomez et al. 2015; 2016), and the characterization of post-treatment engineering properties (Montoya and DeJong 2015), few researchers have investigated the effects of systematic changes in biogeochemical conditions during mineral synthesis on the physical and chemical properties of bio-cemented soils. Past researchers have considered using a diverse range of chemical reagents and concentrations for bio-cementation treatments and while all solutions require urea and calcium, the magnitudes and ratios supplied have varied widely. For example, applied ureato-calcium ratios have varied from 1:1 (Whiffin et al. 2007; van Paassen et al. 2010) to over 100:1 (Ferris et al. 1997; Chou et al. 2011), while concentrations of urea and calcium have spanned from 25 mM to 3000 mM and 2.4 mM to 2000 mM, respectively. Other chemical constituents have been included to control reaction rates, enrich for microbial growth, and alter environmental conditions. At field scale, the ratios and concentrations of these reactants will affect material and energy consumption and may influence material properties and the long-term performance of bio-cemented soils. In addition to the composition of injected solutions, environmental factors including groundwater chemistry and soil mineralogy are largely unavoidable variables with the potential to directly influence chemical conditions during the MICP process. The complex and simultaneous changes in biological, chemical, and physical factors encountered during precipitate synthesis between experiments have blurred the ability of researchers to attribute observations to more specific isolated mechanisms.

In this study, two small-scale batch reactor experiments were conducted to investigate the effect of urea hydrolysis rate and urea and calcium concentration magnitudes on reaction kinetics and precipitate mineralogy and morphology. Small-scale batch reactor experiments were selected for these studies to limit complicating factors related to reactive transport in soils and increase the range of factors that could be practically investigated through minimization of experimental time and materials. In all experiments, equimolar urea-to-calcium concentration ratios were supplied and variations in bulk ureolysis rates were achieved by changing augmented Sporosarcina pasteurii (S. pasteurii) cell densities. During experiments, small volume solution samples were obtained to capture both ureolysis and precipitation kinetics in time through direct urea and calcium measurements. Following experiments, end-state bio-cemented materials were preserved and Scanning Electron Microscopy (SEM) and X-ray Diffraction (XRD) were used to characterize the morphology and mineralogy of synthesized calcium carbonate precipitates. Finally, results from a PHREEQC batch reaction model were compared to experimental data to examine the effect of chemical concentration magnitudes on microbial activity and estimate applied cell densities. Future experiments are expected to address critical knowledge gaps in our understanding of the effect of biogeochemical conditions during precipitation, focusing on factors controlling long-term material performance including crystal morphology, micro-scale distribution, and mineralogy.

MATERIALS AND METHODS

Small Plate Experiments

Small-scale plate batch reactor experiments were selected for these studies to limit complicating factors related to reactive transport in soils and increase the range of factors that could be investigated. All experiments were performed using augmented *S. pasteurii* cell densities to enable urea hydrolysis and the bio-cementation process. Plate experiments were conducted in 35 mm diameter glass petri dishes including 5.0 grams of a poorly-graded Ottawa

F-65 quartz sand ($D_{10} = 0.13$ mm, $D_{60} = 0.23$ mm, no fines) and 44 mL of cementation solution. During experiments, solution samples were obtained in time to capture ureolysis and precipitation kinetics through direct urea and calcium measurements. Following experiments, end-state bio-cemented materials were preserved and Scanning Electron Microscopy (SEM) and X-ray Diffraction (XRD) were used to characterize the morphology and mineralogy of precipitates.

Augmented Cell Cultures

Sporosarcina pasteurii (S. pasteurii) cells (ATCC 11859) were prepared using growth media consisting of 15.74 g/L tris base, 20 g/L yeast extract, and 10 g/L ammonium sulfate, pH-adjusted to near 9.0. Following preparation, growth media was autoclaved at 121°C for 24 minutes and cooled to room temperature before inoculating with a stock S. pasteurii culture stored at -80°C. Inoculated growth media was incubated for 48 hours at 30°C and 175 rpm before harvesting. Concentrated S. pasteurii pellets were created by centrifuging 50 mL of incubated cell media for 10 minutes at 4200 rpm and then pouring off supernatant. The remaining cells were rinsed using an autoclaved isotonic saline solution prepared at 9 g/L (154 mM NaCl), mixed thoroughly, and centrifuged again until the supernatant appeared clear (1 to 3 rinses). A final cell suspension was created by adding 10 mL of isotonic saline to the remaining bacteria and mixing. The OD₆₀₀ of the 10 mL suspension was measured using a microplate spectrophotometer and ranged between 1.5 and 1.6.

Table 1: Summary of Urea and Calcium Concentrations, Ureolytic Rates and Applied Cell Suspensions, Estimated Times to Reaction Completion, and Estimated Augmented Cell Densities for Plate Experiments

	I I						
Plate No.	Equimolar Urea & Calcium Concentrations (mM)	Ureolytic Rate & Applied Cell Suspension (mL)	Estimated Time to Reaction Completion (hours)	Estimated Augmented Cell Densities (cells/mL)			
1	250	Fast (5.5 mL cell suspension)	2	7.0 x 10 ⁷			
2	250	Medium (1.1 mL cell suspension)	10	1.8×10^{7}			
3	250	Slow (0.25 mL cell suspension)	48	3.0×10^6			
4	50	Medium (1.1 mL cell suspension)	8	1.8 x 10 ⁷			
5	500	Medium (1.1 mL cell suspension)	12	1.8×10^7			
6	1250	Medium (1.1 mL cell suspension)	24	1.8×10^{7}			

Bio-cementation Treatments

Prior to starting experiments, 5.0 grams of Ottawa F-65 sand was augmented with the prepared *S. pasteurii* suspension and allowed to reside overnight at 1.6°C to mimic treatment processes wherein soils are first augmented or stimulated to achieve ureolytic activity and then subsequently cemented. For all experiments, 44 mL of cementation solution was then added to the augmented sand, vortexed at 800 rpm for 10 seconds, added to the petri dish, and covered to minimize solution/air interactions. Cementation solutions consisted of equal concentrations of urea (99.2% assay) and calcium chloride dihydrate (>99.0% assay). Upon completion, remaining solutions were collected and frozen for future analysis. Remaining bio-cemented materials were rinsed with 96% (v/v) ethanol and stored in a vacuum desiccator to prevent degradation. For all experiments, solution urea and calcium concentrations, ureolytic rates and applied cell

suspensions, estimated times to reaction completion, and estimated augmented cell densities are summarized in Table 1.

PHREEQC Biogeochemical Model

PHREEQC (Parkhurst and Appelo 2013), a USGS geochemical program, was used to estimate cell densities for all batch experiments by comparing modeled and experimentally measured urea concentrations in time. In this PHREEQC model, microbial ureolysis [Eq. (1)] was modeled using a cell-normalized Michaelis-Menten kinetic rate expression [Eq. (2)] following Lauchnor et al. (2015) wherein d[Urea]/dt is urea hydrolysis rate, [Urea] is urea concentration, [X] is ureolytic cell density, V_{max} is the maximum ureolysis rate per cell, and K_m is the microbial urease enzyme half-saturation coefficient. In this model, enzyme inhibition and all other kinetically-controlled reactions were ignored. Whole cell kinetic parameters reported by Lauchnor et al. (2015) for *S. pasteurii* (ATCC 11859) were implemented in this model where V_{max} was 6.4 x 10⁻⁹ mmol urea cell⁻¹ hour⁻¹ and K_m was 305 mmol 1⁻¹. As shown in Table 1, estimated cell densities for slow, medium, and fast rate experiments ranged from 3 x 10⁶ to 7 x 10⁷ cells per mL.

$$\frac{d[Urea]}{dt} = [X] \left(\frac{V_{max}[Urea]}{K_m + [Urea]} \right)$$
 [Eq. (2)]

Aqueous Sampling

Aqueous solution samples of 120 μ L were collected at pre-determined times during experiments as informed by expected ureolytic rates and the PHREEQC batch reaction model. For all experiments, the total sampled volume never exceeded 10% of the total volume of the solution available (4.4 mL). All aqueous samples were taken near the center of plates using a pipette with disposable polypropylene tips. Samples were then pipetted into a 2.0 mL conical tube with a 0.45 μ m filter and centrifuged at 1318 g for a minimum of 30 seconds to remove all solid precipitates and soil suspended in the solution. 80 μ L of the filtered sample was then added to 300 μ L of 1N hydrochloric acid and mixed thoroughly to prevent volatilization of ammonia and limit the potential for continued ureolytic activity and precipitation reactions. All aqueous samples were frozen immediately after stabilization until subsequent chemical analyses.

Aqueous Chemical Measurements

Aqueous urea measurements were completed using a colorimetric urea assay modified from Knorst et al. (1997) wherein a colorimetric reagent consisting of 4% (w/v) p-Dimethylaminobenzadehyde, and 4% (v/v) HCl in 96% ethanol was added to dilute sample volumes. Absorbance values were measured at 422 nm using a microplate spectrophotometer and compared to calibration relationships. Calcium measurements were completed using a QuantiChrom Calcium Assay Kit (BioAssay Systems). Samples were first diluted to achieve concentrations within the linear range of the assay (< 5.0 mM) and 200 mL of a colorimetric reagent was added and allowed to develop for at least 10 minutes. Absorbance values were measured at 612 nm using a microplate spectrophotometer and compared to calibration relationships.

X-Ray Diffraction Analyses

X-ray Diffraction (XRD) analyses were performed on end-state precipitate materials to characterize their mineralogy, specifically focusing on detecting and quantifying the presence of calcium carbonate polymorphs such as calcite, vaterite, and aragonite. All XRD analyses were performed using a Bruker D8 Discover with IµS 2-D powder XRD system with a high-efficiency Cu anode microfocus x-ray source and Pilatus 100k large-area 2D detector. Scans were performed for 45 seconds for 2Theta (2θ) values from 16 to 93 at increments of 11. Samples were prepared from ethanol-rinsed precipitates obtained from plate experiments and ground into a fine powder using an agate mortar and pestle prior to XRD analyses. Analysis of the obtained diffraction patterns was performed using Diffrac.EVA (Bruker) XRD software.

Scanning Electron Microscope Imaging

Scanning Electron Microscope (SEM) imaging was completed to visually examine morphologies of the precipitated calcium carbonate minerals as well as relative size, shapes, and distribution of calcium carbonate crystals within the bio-cemented sand. SEM imaging was performed using a FEI XL830 Dual-Beam Focused Ion Beam Scanning Electron Microscope. Samples were prepared from ethanol-rinsed precipitates and sputter coated using a 60/40 gold/palladium (Au/Pd) alloy target for 60 seconds at a deposition rate of 13 nm/min in an Argon gas chamber to achieve higher resolution imaging.

RESULTS AND DISCUSSION

Aqueous Chemical Results

Figure 1 presents normalized urea concentrations in time for the slow, medium, and fast ureolytic rate experiments. All experiments received urea and calcium concentrations of 250 mM but contained different cell densities. Although urea measurements show some initial lag in urea hydrolysis and changes in rates over time, a PHREEQC batch reaction model was calibrated to match experimental data for all times less than ≈25 hours by varying supplied cell densities, while assuming whole cell kinetic parameters following Lauchnor et al. (2015) for S. pasteurii. Results suggested that S. pasteurii cell densities varied near 1.5 orders between experiments with 3×10^6 , 1.8×10^7 , and 7×10^7 cells/mL obtained in slow, medium, and fast rate experiments. For the slow ureolytic rate experiment (Figure 1a), the observed rate followed the predicted trend for approximately 30 hours after which it began to significantly slow. The observed reduction in ureolysis rate at late time may have resulted from cell death due to the absence of growth factors and the presence of calcite precipitation in these experiments. Figure 2 presents normalized concentrations of solution soluble calcium and urea measured during ureolysis rate experiments. All experiments began with concentrations of 250 mM urea and calcium. As shown, urea degradation rate increased significantly as the concentration of S. pasteurii cells increased. Similarly, the rate of calcium consumption, indicative of calcium carbonate precipitation, increased as the concentration of cells increased. Similar temporal trends between urea degradation and calcium consumption suggested that the kinetics of microbial ureolysis governed the rate of calcium carbonate precipitation in these experiments.

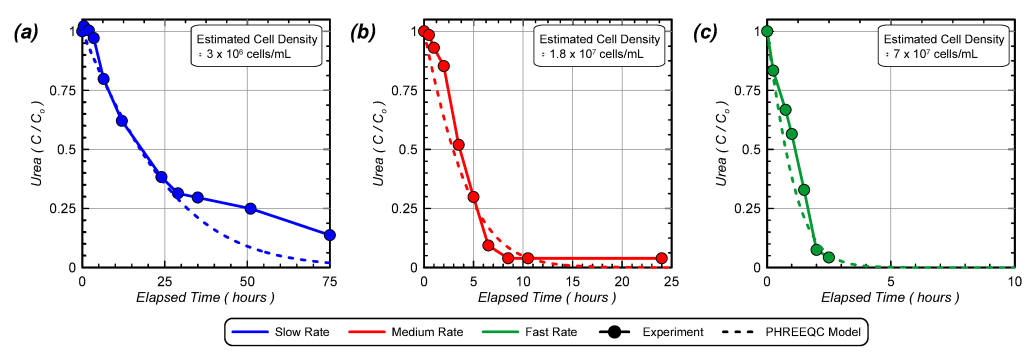


Fig. 1. Normalized concentrations of urea in time for (a) slow, (b) medium, and (c) fast ureolysis rate experiments with calibrated PHREEQC models and estimated cell densities.

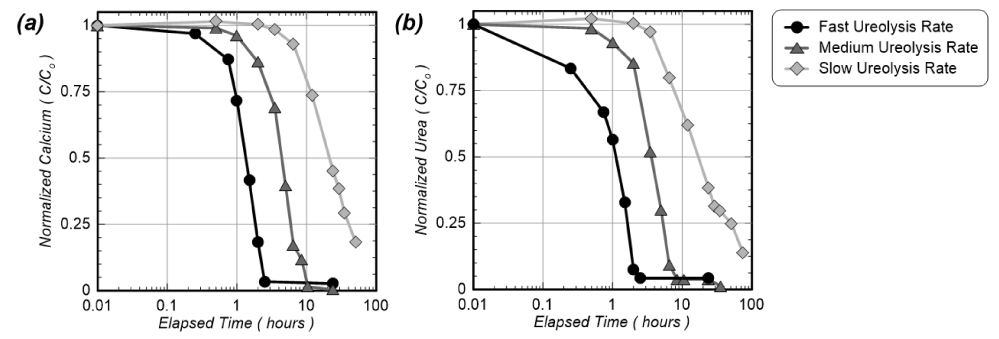


Fig. 2. Normalized concentrations of (a) calcium and (b) urea measured during ureolysis rate experiments.

Figure 3 presents concentrations of soluble calcium and urea in time for chemical concentration experiments wherein 1250 mM, 500 mM, 250 mM, and 50 mM calcium and urea concentrations were applied. When comparing calcium consumption and urea degradation, similar trends in time were again observed, suggesting that urea hydrolysis remained the rate limiting step for CaCO₃ precipitation. In addition, large differences in the time required to achieve full urea hydrolysis and calcium consumption were observed. Due to a much slower ureolysis rate than initially predicted (Table 1), the 1250 mM experiment was terminated before achieving full urea hydrolysis and calcium consumption. Figure 4 presents normalized urea concentrations in time for all chemical concentration varied plate experiments. All chemical concentration experiments were completed using an identical inoculant intended to achieve a medium ureolysis rate. A PHREEQC batch reactor model was used to estimate urea degradation trends in time for each chemical concentration assuming a cell density of 1.8 x 10⁷ cells/mL (from medium rate experiments). This was intended to compare experimentally observed rates to the predicted rate with a stationary cell density acknowledging rate dependencies on applied urea concentrations. For 50 mM (Figure 4d) and 250 mM (Figure 4c) concentrations, the observed rate matched favorably to the PHREEQC modelled trend. At higher chemical concentrations, however, the experimentally observed rate was moderately slower than predicted for the 500 mM experiment (Figure 4b) and substantially slower than that predicted for the 1250 mM experiment (Figure 4a). While it is not fully known why the stationary cell density model significantly overpredicted ureolysis rates at chemical concentrations exceeding 250 mM, several explanations are hypothesized. In addition to possible cell death overtime due to the absence of growth factors (as observed in the slow rate experiment), higher chemical concentrations may have also resulted in greater magnitudes of precipitation and potential "entombment" of cells within crystals as greater quantities of calcium carbonate precipitated. This precipitation may have resulted in cell death, reductions in cellular diffusion, and isolation of cells from bulk aqueous solutions, therefore decreasing the number of cells actively completing urea hydrolysis. At higher chemical concentrations, continued augmentation and/or the addition of growth factors may be required to maintain similar rates of continued ureolysis. Additionally, these results suggest that constant cell density models may be inadequate for accurately predicting urea degradation trends in time when significant precipitation is occurring.

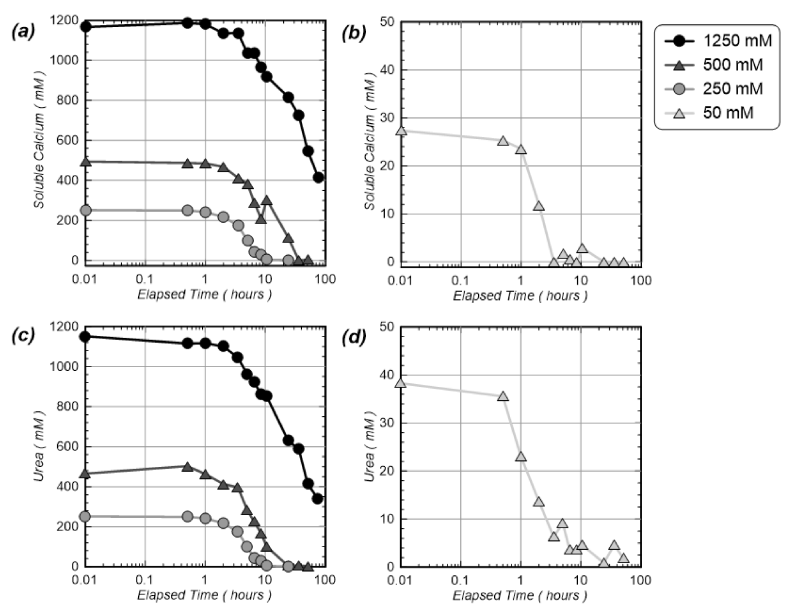


Fig. 3. Concentrations of (a,b) calcium and (c,d) urea in time measured during concentration experiments.

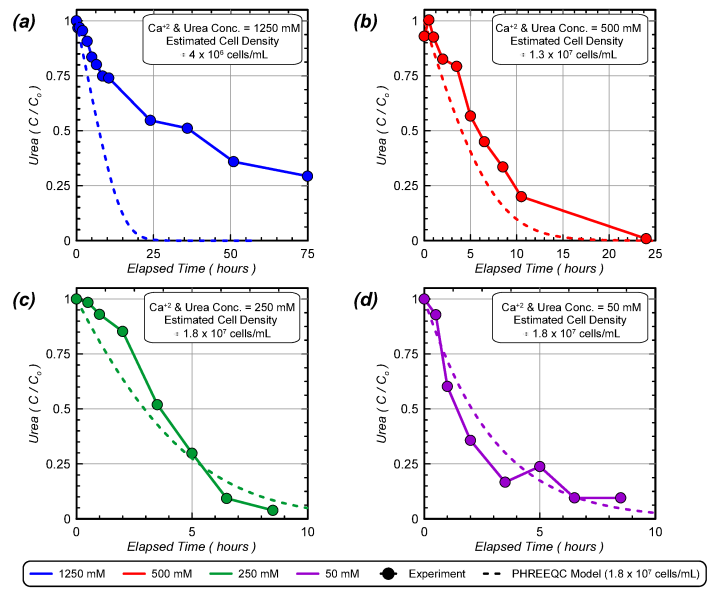


Fig. 4. Normalized urea concentrations in time for (a) 1250 mM, (b) 500 mM, (c) 250 mM, and (d) 50 mM experiments. It should be noted that the estimated cell densities shown match the experimentally observed trends disregarding the similar 1.8×10^7 cells/mL inoculants.

Figure 5 presents comparisons of urea and soluble calcium concentrations measured during ureolytic rate (Figure 5a) and chemical concentration (Figure 5b) plate experiments. Both plots show that most solution samples had urea-to-calcium ratios of less than 1 at any point in time. This result was expected, as urea hydrolysis is required to drive the calcium carbonate precipitation reaction through the production of carbonate species (Mobley et al. 1995). As shown earlier, however, the close association of results with the 1:1 line suggests that while calcium carbonate precipitation appears to be slightly slower than ureolysis, precipitation occurred relatively quickly after urea degradation in all experiments. The rate of calcium carbonate precipitation in these experiments was sufficiently fast that reactions could be reasonably approximated with an equilibrium reaction.

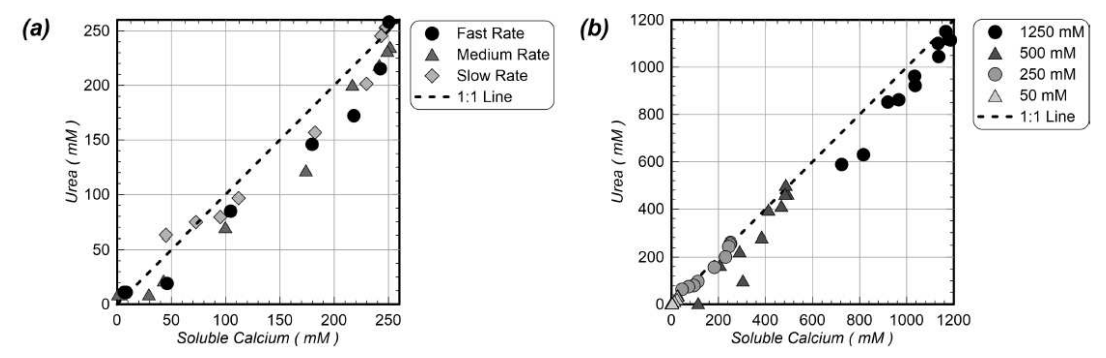


Fig. 5. Comparisons of urea and soluble calcium concentrations during (a) ureolytic rate and (b) chemical concentration experiments.

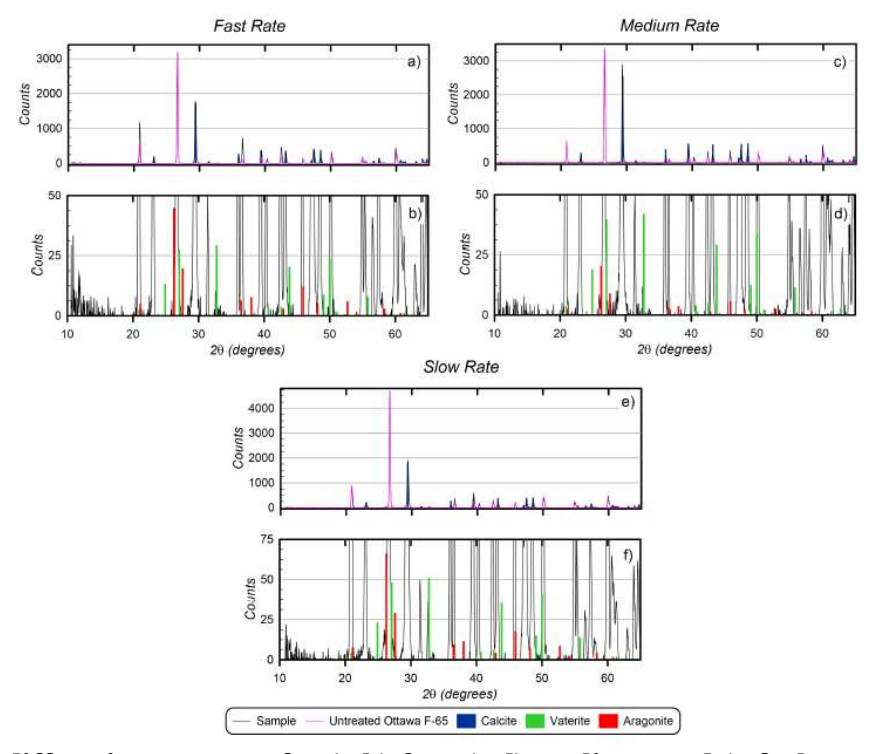


Fig 6. XRD diffraction patterns for (a,b) fast, (c,d) medium, and (e,f) slow ureolytic rate end-state precipitates with scaled diffraction patterns for calcite, vaterite, and aragonite. Magnified XRD diffraction patterns are included to better display vaterite and aragonite patterns.

X-Ray Diffraction Results

Calcium carbonate can exist as several chemically identical but structurally different states or polymorphs. During MICP, the most commonly reported polymorph of calcium carbonate is calcite, however, other polymorphs including vaterite and aragonite may result from biologically-mediated reactions despite being thermodynamically unfavorable. Vaterite and aragonite polymorphs have significantly higher solubilities than calcite in water, and thus the presence of these minerals may have important implications for the long-term performance of bio-cemented soils. In order to assess the presence and relative abundances of these different minerals in end-state precipitate samples, semi-quantitative (S-Q) analyses using Diffrac.EVA software were performed based on reference intensity ratio (RIR) values.

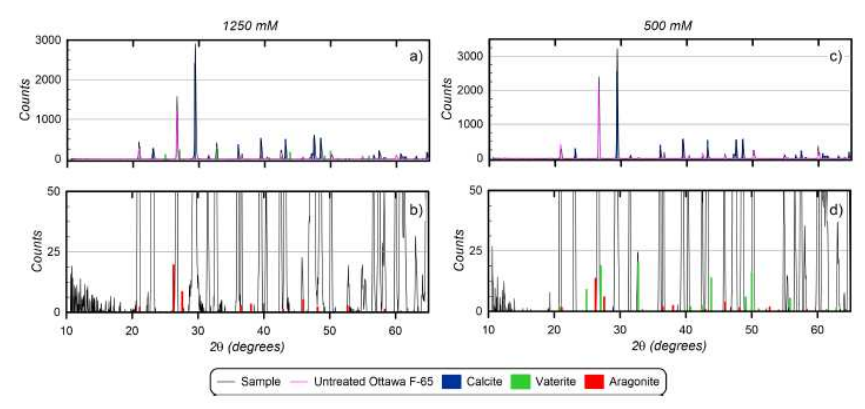


Fig. 7. XRD diffraction patterns for (a,b) 1250 mM, and (c,d) 500 mM end-state precipitates with scaled diffraction patterns for calcite, vaterite, and aragonite. Magnified XRD diffraction patterns are included to better display vaterite and aragonite patterns.

Figure 6 and 7 provide XRD diffraction patterns for ureolytic rate and concentration experiments, respectively. Summaries of the S-Q analysis results for all tests are provided in Table 2. It should be noted that although the lowest concentration experiment (50 mM) did not generate a strong enough diffraction signal to perform a reliable S-Q analysis, the diffraction pattern did suggest the presence of calcite. As shown, XRD analyses suggested that calcite was the predominant polymorph present in all experiments despite varying ureolysis reaction rates and chemical concentrations by orders of magnitude. Relative abundances of calcite detected in ureolysis rate specimens ranged from 83 to 93%, with aragonite and vaterite estimated to be present only in small quantities (2 to 9%). When considering concentration changes, the 500 mM sample showed a dominant calcite phase (96%) with negligible amounts ($\approx 2\%$) of vaterite and aragonite. The 1250 mM sample diffraction pattern also showed that calcite was the most abundant phase, but in smaller quantities (75%) than the other experiments. The presence of vaterite in the 1250 mM sample was detected in significant quantities (23%) by the strong peak at $2\theta = 32.8^{\circ}$ not present in other samples. One possible explanation for the presence of vaterite in this experiment may be that vaterite exists as an intermediate mineral phase during the MICP process and is subsequently transformed into calcite via dissolution and re-precipitation when lower calcium and carbonate concentrations are present at the end of experiments. These lower concentrations can remain super-saturated relative to calcite (lower solubility) but can be undersaturated relative to vaterite (higher solubility), thus inducing vaterite dissolution. This mechanism, known as Oswald ripening, has been shown for many different minerals. Due to a much slower ureolysis rate than expected, the 1250 mM experiment was terminated before all of

the supplied urea and calcium was consumed. This may have allowed solutions to remain supersaturated relative to vaterite at the end of the experiment, possibly leaving it in an intermediate state before dissolution and re-precipitation to calcite could occur at lower calcium and carbonate concentrations.

Table 2. Summary of S-Q Analysis Results Obtained from XRD Diffraction Patterns
XRD Interpreted Compositions

			ARB interpreted compositions		
Plate #	Equimolar Urea/Calcium	Ureolytic Rate	% Calcite	% Vaterite	% Aragonite
	Concentrations (mM)	Oreolytic Nate	By Mass	By Mass	By Mass
1	250	Fast	88	5	7
2	250	Medium	93	2	5
3	250	Slow	83	9	8
4	50	Medium	NA	NA	NA
5	500	Medium	96	2	2
6	1250	Medium	75	23	2

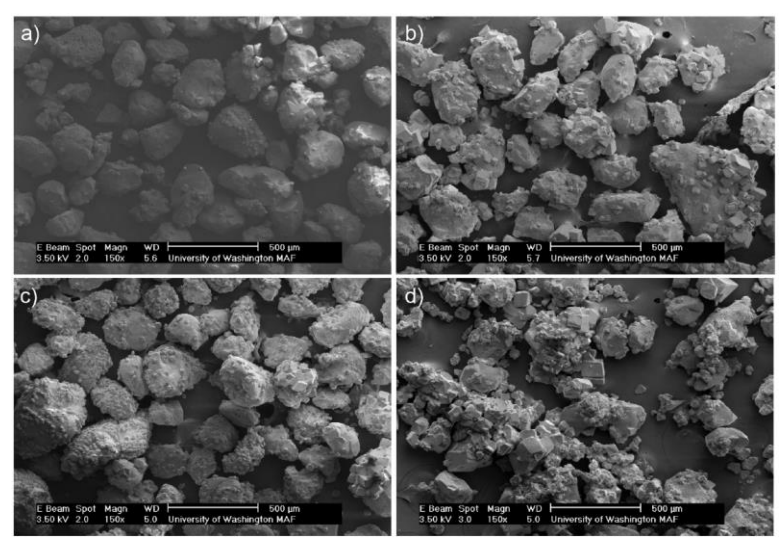


Fig. 8. Representative SEM images of (a) fast, (b) medium, and (c) slow ureolysis rate and (d) 1250 mM concentration end-state precipitate samples at 150x.

SEM Images

Figure 8 shows representative SEM images of the end-state precipitates collected from fast, medium, and slow ureolytic rate experiments and the 1250 mM concentration experiment. When comparing these samples, the fast ureolytic rate precipitate generally showed smaller crystal sizes than the other ureolytic rates. In addition, less of the precipitate appeared to have nucleated on the sand surface. This result was consistent with observations during and after the experiment, which suggested that more precipitation occurred on the surfaces of the plate compared to other ureolytic rate experiments. As expected, the 1250 mM concentration precipitate showed larger crystals and more precipitation on the surface of sand particles, but also differences in precipitate morphologies when compared to the 250 mM experiment performed at the same medium ureolysis rate (Figure 8b). In all samples, most crystal forms appeared consistent with the rhombohedral crystal morphology expected for calcite. Despite XRD analyses suggesting significant vaterite was present in the 1250 mM sample, SEM imaging revealed no obvious spherical crystal morphologies that would be consistent with vaterite. In both the medium rate (250 mM) and 1250 mM specimens, however, crystal morphologies with circular shaped voids

were observed. Past studies have shown that during the Oswald ripening dissolution and reprecipitation processes, calcite crystals can develop and grow while being attached to dissolving vaterite spheres, leaving calcite crystals with vaterite-like casts (Rodriguez, Shaw, Benning 2010). Figure 9 shows three images of calcite crystals with apparent altered morphologies consistent with vaterite casts, which are hypothesized to have resulted from the vaterite-calcite transformation process.

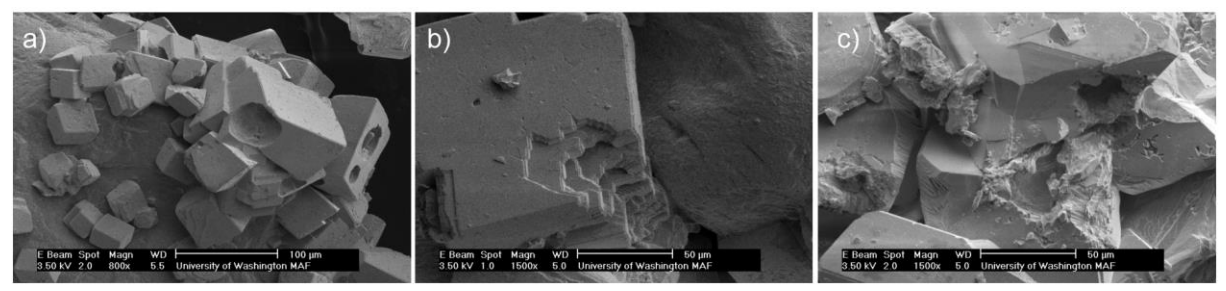


Fig. 9. Images of vaterite casts observed in (a,b) medium rate and (c) 1250 mM experiments.

CONCLUSIONS

Through small-scale batch reactor experiments, the effects of various biogeochemical factors on the MICP process can be isolated and systematically examined. In this study, small-scale batch reactor plate experiments were conducted wherein ureolysis rates and concentrations of supplied urea and calcium were varied to examine their effects on reaction kinetics and precipitate mineralogy and morphology. Chemical assays completed on solution samples in time were used to track urea and calcium concentrations throughout the precipitation process. In all experiments, urea hydrolysis appeared to occur only slightly faster than calcium concentration reductions suggesting that the rates of MICP in these experiments were largely controlled by the kinetics of ureolysis. PHREEQC batch reactor models were used to assess changes in cell densities between rate experiments and explore the effect of chemical concentrations on microbial ureolysis. For low cell concentrations and for urea and calcium concentrations greater than 250 mM, the model predicted faster ureolysis rates than were experimentally observed. This discrepancy may have resulted from cell death in time due to the lack of growth factors and entombment in time resulting from the formation of precipitation surrounding cells. XRD analyses completed on end-state precipitates in all experiments showed an abundance of calcite, with the 1250 mM experiment being the only sample to show significant amounts of vaterite. SEM imaging revealed crystal forms consistent with calcite in all samples; however, some samples displayed crystals with shapes that may indicate that vaterite was present during the precipitation process, but disappeared near the end of experiments due to Oswald ripening processes. While the results of these experiments are promising, future work is needed to verify these results under conditions more representative of subsurface soil materials.

ACKNOWLEDGEMENTS

Funding for this research work was provided by the National Science Foundation (ECI-1824647) and is greatly appreciated. Research collaboration made possible through the Engineering Research Center Program of the National Science Foundation under NSF Cooperative Agreement No. EEC-1449501 is also acknowledged. Part of this work was

conducted at the Molecular Analysis Facility, a National Nanotechnology Coordinated Infrastructure site at the University of Washington which is supported in part by the National Science Foundation (grant NNCI-1542101), the University of Washington, the Molecular Engineering & Sciences Institute, and the Clean Energy Institute. Any opinions, findings, and conclusions or recommendations expressed in this manuscript are those of the authors and do not necessarily reflect the views of the National Science Foundation.

REFERENCES

- Chou, C.W., Seagren, E.A., Aydilek, A.H., & Lai, M. (2011). "Biocalcification of sand through ureolysis." *Journal of Geotechnical and Geoenvironmental Engineering*, 137(12), 1179-1189.
- DeJong, J. T., Fritzges, M. B., & Nüsslein, K. (2006). Microbially induced cementation to control sand response to undrained shear. *Journal of Geotechnical and Geoenvironmental Engineering*, 132(11), 1381-1392.
- DeJong, J.T., et al. (2013). "Biogeochemical processes and geotechnical applications: progress, opportunities and challenges." *Geotechnique*, 63(4), 287-301.
- Ferris, F.; Stehmeier, L.; Kantzas, A.; Mourits, F. (1997) Bacteriogenic mineral plugging. *Journal of Canadian Petroleum Technology*, 36, (09).
- Fujita, Y., Redden, G.D., Ingram, J.C., Cortez, M.M., Ferris, F.G., & Smith, R.W. (2004). "Strontium incorporation into calcite generated by bacterial ureolysis." *Geochimica et Cosmochimica Acta*, 68(15), 3261-3270.
- Gomez, M.G., DeJong, J.T., Anderson, C.M. (2018a). "Effect of Bio-cementation on Geophysical and Cone Penetration Measurements in Sands." *Canadian Geotechnical Journal*.
- Gomez, M.G., Graddy, C.R.M., DeJong, J.T., Nelson, D.C., Tsesarsky, M. (2018b). Stimulation of Native Microorganisms for Bio-cementation at Field Scale Treatment Depths. *Journal of Geotechnical and Geoenvironmental Engineering*, 144(1).
- Gomez, M.G., Anderson, C. M., Graddy, C. M., DeJong, J. T., Nelson, D. C., & Ginn, T. R. (2016). Large-scale comparison of bioaugmentation and biostimulation approaches for biocementation of sands. *Journal of Geotechnical and Geoenvironmental Engineering*, 143(5), 04016124.
- Gomez, M.G., Martinez, B.C., DeJong, J.T., Hunt, C.E., deVlaming, L.A., Major, D.W., & Dworatzek, S.M. (2015). Field Scale Bio-cementation Tests to Improve Sands. *Ground Improvement*, 168(3), pp. 206-216.
- Knorst, M.T., Neubert, R., & Wohlrab, W. (1997). "Analytical methods for measuring urea in pharmaceutical formulations." *Journal of Pharm. and Biomedical Analysis*, 15(11), 1627-1632.
- Lauchnor, E. G., Topp, D. M., Parker, A. E., & Gerlach, R. (2015). Whole cell kinetics of ureolysis by Sporosarcina pasteurii. *Journal of applied microbiology*. 118(6), 1321-1332.
- Minto, J. M., MacLachlan, E., El Mountassir, G., & Lunn, R. J. (2016). Rock fracture grouting with microbially induced carbonate precipitation. *Water Resources Research*, 52(11), 8827-8844.
- Mobley, H. L., Island, M. D., & Hausinger, R. P. (1995). Molecular biology of microbial ureases. *Microbiol. Mol. Biol. Rev.*, *59*(3), 451-480.
- Montoya, B. M., & DeJong, J. T. (2015). Stress-strain behavior of sands cemented by microbially induced calcite precipitation. *Journal of Geotechnical and Geoenvironmental*

- Engineering, 141(6), 04015019.
- Montoya, B. M., DeJong, J. T., & Boulanger, R. W. (2013). Dynamic response of liquefiable sand improved by microbial-induced calcite precipitation. *Géotechnique*, 63(4), 302.
- O'Donnell, S.T., Kavazanjian Jr, E., & Rittmann, B.E. (2017). "MIDP: Liquefaction mitigation via microbial denitrification as a two-stage process. II: MICP *Journal of Geotechnical and Geoenviron*. *Eng.*, 143(12), 04017095.
- Parkhurst, D.L. and Appelo, C.A.J., 2013, "Description of input and examples for PHREEQC version 3--A computer program for speciation, batch-reaction, one-dimensional transport, and inverse geochemical calculations." *U.S. Geological Survey Techniques and Methods*, book 6, chap. A43, 497 p.
- Rodriguez-Blanco, J.D., Shaw, S., & Benning, L.G (2010). "The kinetics and mechanisms of amorphous calcium carbonate (ACC) crystallization to calcite, via vaterite." *Nanoscale*, 2011, 3, 265-271.
- Stocks-Fischer, S., Galinat, J.K., & Bang, S.S. (1999). "Microbiological precipitation of CaCO3." *Soil Biology and Biochemistry*, 31(11), 1563-1571.
- van Paassen, L.A. (2011). Bio-mediated ground improvement: from laboratory experiment to pilot applications. *Geo-Frontiers 2011 Technical Papers*, ASCE, Reston, VA, 4099-4108.
- Whiffin, V.; van Paassen, L.; Harkes, M., Microbial carbonate precipitation as a soil improvement technique. *Geomicrobiology Journal* 2007, 24, (5), 417-423.